Neurochemical Research (2020) 45:278–294
https://doi.org/10.1007/s11064-019-02912-3

ORIGINAL PAPER

Involvement of PARP-1/AIF Signaling Pathway in Protective Effects of Gualou Guizhi Decoction Against Ischemia–Reperfusion Injury-Induced Apoptosis

Lihong Nan[1] · Qingqing Xie[2] · Zheming Chen[3] · Yuqin Zhang[1] · Yaping Chen[1] · Huang Li[1] · Wenfang Lai[1] · Yan Chen[1] · Mei Huang[1]

Received: 1 July 2019 / Revised: 8 November 2019 / Accepted: 16 November 2019 / Published online: 2 December 2019

Abstract

Cerebral ischemia–reperfusion injury is a complex pathophysiological process. Poly(ADP-ribose) (PAR) polymerase-1 (PARP-1)/apoptosis-inducing factor (AIF) signaling pathway-mediated apoptosis is one of the non-caspase-dependent cell death programs that are widely present in neurological diseases such as stroke. In our study, we aimed to conduct further research on the effects of Gualou Guizhi decoction (GLGZD) on the PARP-1/AIF signaling pathway in cell apoptosis after ischemia–reperfusion injury caused by middle cerebral artery occlusion (MCAO). The results showed that GLGZD administration for 7 days significantly ameliorated MCAO-induced neurological damage, limb paralysis and the pathological state of the ischemic cortex. GLGZD exerted its effects by significantly reducing the volume of ischemic cerebral infarction, increasing the number of Nissl-positive cells, and reducing neuronal apoptosis. Furthermore, Western blot analysis showed that GLGZD significantly inhibited the total protein expression of PARP-1, PAR, AIF and endonuclease G (Endo G) in the ischemic cortex and significantly increased the total protein expression of heat-shock protein 70 (Hsp70). On the one hand, the expression of PARP-1, AIF and Endo G protein in the nucleus significantly decreased while the expression of PAR nucleoprotein significantly upregulated. On the other hand, compared with the MCAO model group, the GLGZD-treated group showed a significantly reduced protein expression of PAR in mitochondria and significantly increased protein expression of mitochondrial AIF and Endo G. It was concluded that GLGZD had good therapeutic effects in MCAO model rats. These effects were closely related to GLGZD-mediated inhibition of ischemia-induced neuronal apoptosis by regulation of protein expression and translocation in the PARP-1/AIF signaling pathway.

Keywords Gualou Guizhi decoction · Focal cerebral ischemia · Poly(ADP-ribose) polymerase-1 · Poly(ADP-ribose) · Apoptosis-inducing factor

Introduction

Stroke has the characteristics of high morbidity, high disability, high mortality and high recurrence rate. It is a kind of common disease that seriously threaten to the human health [1]. In recent years, the incidence of stroke has increased annually, and there has been a trend toward younger patients [2]. Stenosis or occlusion of the cerebral artery may lead to various sequelae after stroke, including neurological dysfunction. Among these sequelae, motor dysfunction is the most serious, with approximately 80–90% of stroke patients with hemiplegia experiencing limb spasticity of different degrees [3], which limits their activity. Some patients suffer irreversible secondary complications due to joint stiffness caused by increased muscle tone [4]. These secondary

Lihong Nan and Qingqing Xie are Co-first authors.

All authors have contributed equally to this study.

✉ Mei Huang
hmei0303@qq.com

[1] College of Pharmacy, Fujian University of Traditional Chinese Medicine, Fuzhou 350122, Fujian, China

[2] Hangzhou Simo Co., Ltd., Nanjing 210001, Jiangsu, China

[3] Pharmaceutical Preparation Section, Quanzhou First Hospital, Quanzhou 362000, Fujian, China

complications seriously affect the patients' motor function and daily life, further limiting their recovery. Therefore, limb spasticity after stroke is a major problem that needs to be solved during the rehabilitation of stroke.

It is currently believed that limb spasticity after stroke is caused by upper motor neuron injury after cerebral ischemia. Because apoptosis is the main form of cell injury in the penumbra surrounding the infarct area after ischemia–reperfusion injury, apoptosis is regarded as the main form of neuronal loss caused by cerebral ischemia and is closely related to the expansion of the infarct area [5, 6]. Apoptosis is a genetically controlled cell death program. It is delayed and reversible. Slowing and preventing apoptosis gives the therapeutic opportunities for inhibiting the ischemic process, allowing for time to administer drugs to alleviate neuronal injury and even reduce the infarct area [7, 8].

Drug therapy is the first-line intervention for stroke. Inhibition of neuronal ischemic apoptosis is one of the important strategies for stroke rehabilitation [9, 10]. In recent years, many studies have reported that poly (ADP-ribose) (PAR) polymerase-1 (PARP-1)/apoptosis-inducing factor (AIF) signaling pathway-mediated apoptosis is a caspase-independent cell death program. This process, named parthanatos (PARP-1-dependent apoptosis) by Harraz [11], PARthanatos is regarded as the main mechanism to mediate glutamate-induced excitotoxicity, which mediated apoptosis in a caspase-independent cell death program. This process is mediated by the damage of DNA, PARP-1 over activation, increased PAR production and the translocation of AIF from mitochondria to the nucleus [12]. PARthanatos widely existed in neurological diseases like ischemic stroke [13], PARP-1/AIF signaling pathway provides new approaches and targets for the treatment of ischemic stroke.

Chinese medicine has a long history of treating stroke and its sequelae. Gualou Guizhi decoction (GLGZD), reported by Zhang Zhongjing in JinKui YaoLue (a traditional Chinese medical work), consists of 6 kinds of Chinese herbs: *Trichosanthes kirilowii* Maxim., *Cinnamomum cassia* Presl., *Paeoniae lactiflora* Pall., *Zingiber officinale* Rosc., *Ziziphus jujuba* Mill. and *Glycyrrhiza uralensis* Fisch. GLGZD is mainly used for the treatment of limb spasticity after stroke and spinal cord injury [14, 15]. Our previous study revealed that GLGZD exerts its neuroprotective effects by various mechanisms, such as regulating the activity of excitatory glutamate levels and inhibiting the expression of glutamate receptors (α-amino-3-hydroxy-5-methylisoxazole-4-propionic acid receptors and N-methyl-D-aspartic acid receptors) [16–20].

Numerous studies have confirmed that PARP-1 overexpression after cerebral ischemia plays an important role in aggravating nervous system injury and that PARP-1 is closely related to non-caspase-dependent apoptosis. However, whether GLGZD exerts neuroprotective effects by regulating this molecular mechanism has not been declared. Therefore, our study established a rat model of middle cerebral artery occlusion (MCAO) to observe the therapeutic effects of GLGZD on MCAO-injured rats and to explore the mechanism by which GLGZD alleviates limb spasticity after stroke. In addition, we further investigated whether GLGZD inhibited neuronal apoptosis caused by cerebral ischemia by regulating the PARP-1/AIF signaling pathway. This study provides a scientific basis for academic research as well as novel insights into the clinical application of GLGZD for neurological rehabilitation after stroke.

Materials and Methods

Chemicals and Reagents

Standard substances, including citrulline, gallic acid, protocatechuic acid, oxypaeoniflorin, vanillic acid, albiflorin, paeoniflorin, ethyl gallate, schaftoside, neoliquiritin, liquiritin, liquiritin apioside, pentagalloylglucose, isoliquiritin apioside, isoliquiritin, neoisoliquiritin, glycyrrhizin, cinnamic acid, allocinnamic acid, benzoyl paeoniflorin, isoliquiritigenin, glycyrrhizic acid, 6-gingerol, curcumin, licochalcone A, and glycyrrhetinic acid, were purchased from the China Pharmaceutical and Biological Products Institute (Beijing, China). Chromatographic grade methanol and acetonitrile were purchased from Merck (Darmstadt, Germany).

Plant Materials

Trichosanthes kirilowii Maxim., *Cinnamomum cassia* Presl., *Paeoniae lactiflora* Pall., *Zingiber officinale* Rosc., *Ziziphus jujuba* Mill. and *Glycyrrhiza uralensis* Fisch. were all purchased from Beijing Tong Ren Tang Chinese Medicine Co., Ltd. All Chinese herbs were appraised by Professor Yang Chengzi and deposited at the College of Pharmacy, Fujian University of Traditional Chinese Medicine.

Animals

Male Sprague–Dawley rats (weighing 210–230 g) were obtained from the Experimental Animal Center of Zhejiang Province (License: SCXK (Zhe) 2014-0001) (Zhejiang, China) and housed in the animal maintenance facility at the Experimental Animal Center of Fujian University of Traditional Chinese Medicine. A 12 h light/dark cycle was used throughout the experiment, and food and water were provided ad libitum during the experiment. All animal treatments were conducted in strict accordance with international ethics guidelines and the National Institutes of Health's Guide for the Care and Use of Laboratory Animals. The experiments were performed after adaptive feeding for

7 days and approved by the Ethics Committee of Fujian University of Traditional Chinese Medicine (Fuzhou, China).

Preparation of the GLGZD

According to the original prescription of "Jinkui Yaolue", 30 g of *Trichosanthes kirilowii* Maxim, 9 g of *Cinnamomum cassia* Presl, 9 g of *Zingiber officinale* Rosc, 6 g of *Ziziphus jujuba* Mill, 9 g of *Paeoniae lactiflora* Pall, and 6 g of *Glycyrrhiza uralensis* Fisch were weighed. The medicinal material was crushed, extracted twice respectively with 10 times and 8 times volume of ultrapure water for 1.5 h by a reflux process, and filtered. The filtered GLGZD aqueous extract was collected and combined, and then concentrated to a final concentration of 1.44 g/mL by a rotary evaporator.

HPLC Analysis of GLGZD

Compounds in GLGZD were analyzed by Shimadzu HPLC system coupled with a photodiode array detector (Kyoto, Japan). The HPLC system included an ALC-20A pump, a DGU-20A5 degasser, an SIL-20A autoinjector, and a CTO-20A column thermostat. Dikma diamond C18 (250 × 4.6 mm, 5 μm) was used for chromatographic separation, and its working temperature was maintained at 30 °C. The mobile phase was 0.1% formic acid aqueous solution (A) and acetonitrile (B) with a gradient elution program as follows: 0–8 min, 5% B; 8–50 min, 5–35% B; 50–65 min, 35–50% B; 65–75 min, 50–60% B; 75–85 min, 60–70% B; 85–100 min, 70–90% B. The flow rate was kept at 0.8 mL/min, and the injection volume was set at 10 μL.

Muscle Tension Grade

The muscle tension score, which was based on the modified Ashworth muscle tension grade [21], was assessed as follows: grade of 0, no increase in muscle tension and the rats can move freely; grade of 1, slightly increased muscle tension with catch and release during flexion or extension; grade of 2, obvious increase in muscle tension, but the limbs are still prone to flexion and extension and there is mild ataxia; grade of 3, significantly increased muscle tension and difficulty in passive activity as well as moderate ataxia in the rats; grade of 4, limited limb flexion and extension as well as severe ataxia. A muscle tension grade ≥ 1 indicated the presence of limb spasm.

MCAO Model Establishment

The rats were fasted for 12 h with a continual supply of water. Then, 12 rats were randomly selected as the sham operation control group, and the remaining rats were assigned to the model group. After the rats were anesthetized with an intraperitoneal injection of 2% sodium pentobarbital (60 mg/kg), the left common carotid artery, external carotid artery and internal carotid artery were separated and exposed. A 3-0 silicon rubber-coated nylon monofilament was inserted into the proximal part of the middle cerebral artery from the left middle carotid artery. At this point, the MCAO filament was inserted until a light resistance was felt. The dark spot of the filament was situated in the common carotid artery bifurcation (approximately 18 mm). After embolization for 2 h, the filament was pulled out, allowing for reperfusion. Rats in the sham operation control group underwent a neck dissection and coagulation of the arteries, but the nylon monofilament was not inserted to occlude the middle cerebral artery. The specific operation was conducted according to recently reported protocols [16]. when the rats were awake naturally after operation, the neurological function scores were evaluated immediately according to Zea Longa's scoring criteria [22] as follows: score of 0, free activity and no neurological symptoms; score of 1, unable to stretch the contralateral forelimb; score of 2, contralateral forelimb flexion; score of 3, rotating and slightly falling to the contralateral side while crawling; score of 4, severely falling to the opposite side when waking; score of 5, contralateral paralysis, unable to walk without assistance or unconscious. The muscle tension grading was performed immediately after obtaining the neurobehavioral score. The scoring process was performed in a double-blind manner, and was completed simultaneously and independently by two experimenters who had not taken part in the experiments and were familiar with the scoring criteria. The rats with a neurological deficit scores of 3 to 4 and a muscle tension grade ≥ 1 in MCAO group and the rats in sham group were further calculated the cerebral infarction volume in small animal magnetic resonance imager (MRI, Bruker Medizintechnik, Karlsruhe, Germany) of T2 weight imaging (T2WI) sequence scanning. The cerebral infarction volume of MCAO rats were calculated to ensure the success establishment of MCAO model. Rats with cerebral infarction volume of 20–45% were used for the further experiments. The parameters of MRI were set as follows: T2WI was in TSE sequence; Repetition Time: 4200 ms; Echo Time: 35 ms; Number of slices: 21; Field of view: 32 mm × 32 mm; Number of Signal Averaged: 2; acquisition time: 4 min 28 s 800 ms.

Groups and Administration

In the sham-operated group (n = 12), after the sham operation, an equal volume of saline was administered intragastrically daily. Rats with successful modeling were randomly divided into 4 groups. In the MCAO group (n = 12), after MCAO modeling, an equal volume of saline was administered intragastrically daily. In the GLGZD low-dose group (GLGZD-L, n = 12), after MCAO modeling, rats were

administered GLGZD (3.6 g/kg) intragastrically daily at 1 mL/100 g. In the GLGZD middle-dose group (GLGZD-M, n = 12), after MCAO modeling, rats were administered GLGZD (7.2 g/kg) intragastrically daily at 1 mL/100 g. In the GLGZD high-dose group (GLGZD-H, n = 12), after MCAO modeling, rats were administered GLGZD (14.4 g/kg) intragastrically daily at 1 mL/100 g. All of the administrations mentioned above were performed once a day for 7 days.

Modified Neurological Severity Score (mNSS)

After 7 days of treatment with GLGZD, the neurologic deficits of the rats were evaluated by the mNSS [23] which includes four parts: motor tests (raising the mouse by the tail, placing rat on the floor), sensory tests (placing test and proprioceptive test), beam balance tests, reflex tests and an assessment of abnormal movements. The scoring process was performed in a double-blind manner, and was completed simultaneously and independently by two experimenters who had not taken part in the experiments and were familiar with the scoring criteria. The assessment was performed on a scale of 0 to 18 (0: normal score; 18: maximal deficit score). The muscle tension grading was performed immediately after obtaining the mNSS.

Detection of Motor Function in Rats

The motor function of rats was assessed by the CatWalk gait analysis system (XT10.0, Noldus Information Technology Co.,Ltd, Wageningen, Netherlands), and the experiment was carried out in a dark room. Each rat underwent pretraining to pass through the Catwalk glass plate within 10 s without stopping. The rats' foot prints were captured by CatWalk XT to visualize the prints and calculate the print dimensions including the run average speed, the run duration, print area and stride length.

Hematoxylin and Eosin (HE) Staining

One hour after the last administration, the rats were anesthetized by intraperitoneal injection of 2% sodium pentobarbital (60 mg/kg). The thoracic cavity was opened to expose the heart. The perfusion needle was inserted from the apex of the heart to the left ventricle, and the right atrial appendage was cut to form a perfusate. Then, the rats were transcardially perfused with 300 mL of cold saline solution, followed by 300 mL of precooled 4% paraformaldehyde. After perfusion, the brains were removed and postfixed in 4% paraformaldehyde for 24 h, paraffin-embedded, sliced at 5 μm, dewaxed to water, and stained with HE. Pathological changes in the brain tissue were observed under an optical microscope (Leica, Wetzlar, Germany).

2,3,5-Triphenyl-2H-Tetrazolium Chloride (TTC) Staining

One hour after the last administration, rats were anesthetized and decapitated, and the brains were quickly excised. The olfactory bulb, cerebellum and lower brain stem were removed. The remaining portion was cooled in a refrigerator at − 20 °C for 20 min before being used. Rat stainless steel brain matrices were used to cut 2-mm slices in both the front and back of the optic chiasma. The sections were placed in TTC solution (Sigma, St. Louis, MO, USA) for 30 min at 37 °C in the dark, and the brain slices were flipped every 10 min to ensure that they were evenly dyed. Images were taken with a digital camera (Canon, Tokyo, Japan), and the infarct volume ratio was measured and analyzed with ImageJ 1.37 image analysis software (Bethesda, MD, USA).

Nissl Staining

The brain sections were dewaxed and stained by a preheated 0.5% toluidine blue aqueous solution (Nanjing Senbeijia Biotechnology Co., Ltd., Nanjing, Beijing) at 57 °C for 20 min. The sections were rinsed with distilled water and differentiated in 95% ethanol. After blotting and drying, to evaluate the expression of Nissl bodies, images were obtained at a magnification of × 400. Five fields per slice in each group were used to analyze the number of Nissl-positive cells (that is, the number of intact neurons) by Image J 1.37 software (Bethesda, MD, USA).

Terminal Deoxynucleotidyl Transferase-Mediated DUTP-Biotin Nick-End Labeling (TUNEL) Analysis

Five-micrometer paraffin sections were routinely dewaxed, rinsed twice with PBS, fixed in 4% paraformaldehyde for 15 min, and washed 3 times with PBS for 5 min each time. The sections were placed in a box; next, 100 μL of proteinase K working solution was added to each slice, and the samples were incubated for 10 min at room temperature. The slices were fixed again in 4% paraformaldehyde for 5 min, and washed in PBS 3 times for 5 min each time. Then, 100 μL of equilibration buffer was added to each slice, and the slices were equilibrated for 5 min at room temperature; the equilibration buffer was carefully aspirated from the edges with absorbent paper. Then, 51 μL of a TdT enzyme reaction solution (Promega, Wisconsin, USA), which contained 45 μL of equilibration solution, 5 μL of nucleoside mixture and 1 μL of rTdT enzyme, was added to the slices in the dark. The tissue slices were covered with parafilm, placed in a black humidified chamber, and incubated at 37 °C for 1 h in the dark. Next, the parafilm was removed, and the tissue slices were immersed in 2 × sodium citrate buffer for 15 min at room temperature to stop the reaction and then

washed with PBS 3 times for 5 min each time. Then, 100 μL of DAPI dye solution (Beyotime Biotechnology, Beijing, China) was added to dye the nuclei for 8 min in the dark at room temperature; next, the slices were washed with PBS 3 times for 5 min each time. Then, half drop of anti-quenching agent was added, and the slides were covered and kept in the dark. The staining results were observed under a laser confocal microscope (LSM710, CARL ZEISS, Oberkochen, Germany). Apoptotic cells were stained green after TUNEL staining and analyzed by Image J 1.37 software (Bethesda, MD, USA) to calculate the TUNEL-positive expression rate as follows: TUNEL-positive expression rate = (TUNEL-positive cells/nuclear DAPI-positive cells) × 100%.

Immunofluorescence Analysis

Five-micrometer paraffin sections were routinely dewaxed to water, incubated with 3% H_2O_2 to inhibit endogenous peroxidase activity, and subjected to antigenic repair by the microwave method. The sections were then incubated with goat serum working solution for 2 h at room temperature, followed by incubation with anti-PARP-1 rabbit polyclonal antibody (1:600, Santa Cruz, CA, USA) overnight at 4 °C. Twenty-four hours later, the primary antibodies were removed by washing the sections in PBS, and then the sections were incubated with goat anti-rabbit IgG fluorescent secondary antibody (1:1000, Thermo Fisher Scientific, MA, USA) for 1.5 h at room temperature in the dark. The DAPI dye solution was added to stain nuclei for 8 min at room temperature. Half drop of anti-quenching agent was added to cover the tissue slices. A laser scanning confocal microscope was used for observation under 400 × magnification. ImageJ 1.37 software (Bethesda, MD, USA) was used to analyze the number of positive cells in 5 different parts of each section from each group.

Isolation of Total Protein, Nucleoprotein and Mitochondrial Protein

One hour after the last administration, the rats were anesthetized and decapitated. The brain was quickly excised, and the removed brain tissue was placed in a Petri dish on an ice tray. The ischemic cortex was isolated and quickly placed in liquid nitrogen. The samples were then transferred to a − 80 °C refrigerator for storage. The tissue mentioned above was ground to powder in a mortar to acquire the total protein, nucleoprotein and mitochondrial protein, and liquid nitrogen was added without interruption during the grinding. The specific extraction method was as follows:

(1) Total protein extraction: One hundred milligrams of the tissue powder mentioned above was placed into precooled 1.5 mL enzyme-free EP tubes. Then, 1 mL of RIPA lysis buffer containing 1 mM phenylmethanesulfonyl fluoride (Beyotime, Beijing, China) was added, and the tubes were placed on ice for 30 min. The samples were centrifuged at 4 °C and 14,000 × *g* for 30 min in a high-speed cryogenic centrifuge (Eppendorf, Hamburg, Germany). The supernatant was collected to obtain total protein. (2) Nucleoprotein extraction: One hundred milligrams of the tissue powder mentioned above was placed into precooled 1.5 mL enzyme-free EP tubes. Immediately, 1 mL of cytosolic extraction reagent (Boster Biological Technology Co., Ltd., Wuhan, China) was added and mixed for 5 s with high speed and intense agitation. The samples were then centrifuged using a high-speed cryogenic centrifuge (Eppendorf, Hamburg, Germany) at 4 °C and 16,000 × *g* for 10 min. The supernatant was removed, and 200 μL of the nuclear extraction reagent was added (Boster Biological Technology Co., Ltd., Wuhan, China), followed by vortexing for 15 s to ensure complete suspension and dispersal. Then, after incubation on ice, vortexing was performed for 20 s every 5 min for a total of 30 min. Subsequently, the samples were centrifuged in a high-speed cryogenic centrifuge (Eppendorf, Hamburg, Germany) at 4 °C and 16,000 × *g* for 10 min to collect the nucleoprotein extraction. (3) Mitochondrial protein extraction: One hundred milligrams of the tissue powder mentioned above was placed into precooled 1.5 mL enzyme-free EP tubes. Then, 1.5 mL of precooled lysate 1 (Boster Biological Technology Co., Ltd, Wuhan, China) was immediately added and the mixture was agitated and mixed for 20 s. The samples were then centrifuged by a high-speed cryogenic centrifuge (Eppendorf, Hamburg, Germany) at 4 °C and 800 *g* for 5 min. Next, 0.5 mL of the supernatant was added to 0.5 mL of precooled mitochondrial extraction reagent (Boster Biological Technology Co., Ltd, Wuhan, China) in a non-enzyme EP tube. The mixture was centrifuged at 4 °C and 15,000 × *g* for 10 min, and the mitochondria were precipitated. Next, the precipitates were rinsed with 0.2 mL of PBS and then centrifuged at 4 °C and 15,000 × *g* for 10 min. The supernatant was discarded, and 200 μL of precooled lysate 2 (working solution) was added. Agitation was performed on a 4 °C rocking platform for 15 min, and the samples were centrifuged at 4 °C and 12,000 × *g* for 15 min to obtain the supernatant containing the mitochondrial proteins.

Western Blot Analysis

After protein extraction, the protein concentration of each sample was determined by the BCA method. The protein sample was boiled at 100 °C for 10 min, and each sample (50 μg total protein) was separated with 10% sodium dodecyl sulfate–polyacrylamide gel electrophoresis (SDS-PAGE) and then transferred to a nitrocellulose (NC) membrane. The transferred NC membrane was blocked for 2 h with 5% skim milk powder in Tris-buffered saline with

0.1% Tween-20 (T-TBS). The membranes were then incubated with anti-PARP-1 rabbit polyclonal antibody (1:500, Santa Cruz, CA, USA), anti-AIF rabbit monoclonal antibody (1:500, Abcam, Cambridge, UK), anti-PAR rabbit polyclonal antibody (1:500, Abcam, Cambridge, UK), anti-Endo G rabbit polyclonal antibody (1:500, Abcam, Cambridge, UK), anti-Hsp70 mouse monoclonal antibody (1:1000, Abcam, Cambridge, UK), anti-β-actin mouse monoclonal antibody (1:1000, Beyotime Biotechnology, Shanghai, China), anti-histone H3 mouse monoclonal antibody (1:1000, Beyotime Biotechnology, Shanghai, China), or anti-Cox IV small murine monoclonal antibody (1:1000, Beyotime Biotechnology, Shanghai, China) overnight on a 4 °C side-to-side shaker with gentle shaking. After rinsing, the following secondary antibodies were added: goat anti-mouse IgG (1:3000, Thermo Fisher Scientific, MA, USA), goat anti-rabbit IgG (1:3000, Thermo Fisher Scientific, MA, USA), and donkey anti-goat IgG (1:5000, Abcam, Cambridge, UK). The membrane was incubated for 2 h at room temperature on a pendulum shaker with gentle shaking. ECL staining was performed after rinsing, and the signal of the proteins was detected in a gel imaging system (Bio-Rad, CA, USA). ImageJ software was applied to analyze gray values quantitatively. β-actin was regarded as the internal reference protein for total protein. Histone H3 was regarded as an internal reference protein for nucleoprotein, and Cox IV was used as the internal reference protein for mitochondrial protein. The relative expression of the target protein = the gray value of the target protein/the gray value of the internal reference protein.

Statistical Analysis

All results are expressed as the mean ± SD, and the experimental data were statistically analyzed by SPSS 20.0 software (Chicago, IL, USA). Except for the statistical analysis of the data in the neurological function scores and muscle tension score was performed by Kruskal–Wallis test, the rest of statistical analysis was performed by independent samples *t* test, one-way analysis of variance (ANOVA) was followed by Least Significant Difference (LSD) test when equal variance was assumed or by Games–Howell test when equal variance was not assumed. The values of $P < 0.05$ were considered statistically significant.

Results

Qualitative and Quantitative Analysis of GLGZD by HPLC

The main components of GLGZD were qualitatively and quantitatively analyzed by HPLC to acquire the chromatographic fingerprint (Fig. 1). The main 26 compounds in GLGZD and their concentrations detected by HPLC were as follows: citrulline 4.09 mg/g, gallic acid 0.51 mg/g, protocatechuic acid 0.04 mg/g, oxypaeoniflorin 0.07 mg/g, vanillic acid 0.04 mg/g, albiflorin 2.50 mg/g, paeoniflorin 4.50 mg/g, ethyl gallate 0.03 mg/g, schaftoside 0.30 mg/g, neoliquiritin 0.22 mg/g, liquiritin 0.55 mg/g, liquiritin apioside 0.21 mg/g, pentagalloylglucose 0.53 mg/g, isoliquiritin apioside 0.18 mg/g, isoliquiritin 0.21 mg/g, neoisoliquiritin

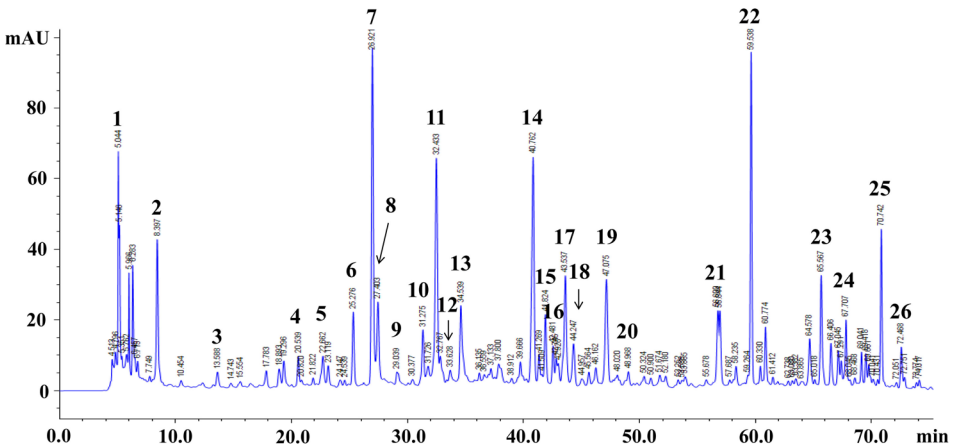

Fig. 1 Fingerprint of the Gualou Guizhi decoction (GLGZD). (1) citrulline 4.09 mg/g, (2) gallic acid 0.51 mg/g, (3) protocatechuic acid 0.04 mg/g, (4) oxypaeoniflorin 0.07 mg/g, (5) vanillic acid 0.04 mg/g, (6) albiflorin 2.50 mg/g, (7) paeoniflorin 4.50 mg/g, (8) ethyl gallate 0.03 mg/g, (9) schaftoside 0.30 mg/g, (10) neoliquiritin 0.22 mg/g, (11) liquiritin 0.55 mg/g, (12) liquiritin apioside 0.21 mg/g, (13) pentagalloylglucose 0.53 mg/g, (14) isoliquiritin apioside 0.18 mg/g, (15) isoliquiritin 0.21 mg/g, (16) neoisoliquiritin 0.11 mg/g, (17) glycyrrhizin 0.36 mg/g, (18) cinnamic acid 0.14 mg/g, (19) allocinnamic acid 0.23 mg/g, (20) benzoyl paeoniflorin 0.08 mg/g, (21) isoliquiritigenin 0.07 mg/g, (22) glycyrrhizic acid 4.23 mg/g, (23) 6-gingerol 0.07 mg/g, (24) curcumin 0.03 mg/g, (25) licochalcone A 0.20 mg/g, (26) glycyrrhetinic acid 0.03 mg/g

0.11 mg/g, glycyrrhizin 0.36 mg/g, cinnamic acid 0.14 mg/g, allocinnamic acid 0.23 mg/g, benzoyl paeoniflorin 0.08 mg/g, isoliquiritigenin 0.07 mg/g, glycyrrhizic acid 4.23 mg/g, 6-gingerol 0.07 mg/g, curcumin 0.03 mg/g, licochalcone A 0.20 mg/g, and glycyrrhetinic acid 0.03 mg/g.

Nerve Function Damage, Muscle Tension and Cerebral Infarction Volume in MCAO-Injured Rats Before GLGZD Treatment

As shown in Fig. 2a–d, in the sham group, there were no neurological impairment symptoms and cerebral infarction lesions, the neurological deficit scores and muscle tension scores were 0. Compared with the sham group, the MCAO group and GLGZD-untreated groups had a significantly increased neurological function score, muscle tension score and cerebral infarction volume ($P < 0.01$). These groups showed cerebral infarction lesions, suggesting that the limb-spasm rat model of MCAO was successfully established. The neurological deficit score, muscle tension score and cerebral infarction volume were not significantly different among these groups before GLGZD treatment.

Effects of GLGZD on Nerve Function Damage, Muscle Tension and Cerebral Infarction Volume in MCAO-Injured Rats

There were no neurological impairment symptoms in the sham group, and the mNSS and muscle tension scores were 0 (Fig. 3a, b). The TTC staining results showed that when the slices from the sham group were stained with rose-carmine, no infarction was found (Fig. 3c, d). Compared with those in the sham group, the mNSS, muscle tension score and cerebral infarction volume increased significantly in MCAO group ($P < 0.01$), and the cerebral infarction area was not stained and appeared white. These results suggested that MCAO was successfully established. The mNSS, muscle tension score and cerebral infarction volume of MCAO-injured rats treated with GLGZD were significantly lower than those of rats subjected to MCAO alone ($P < 0.05, 0.01$).

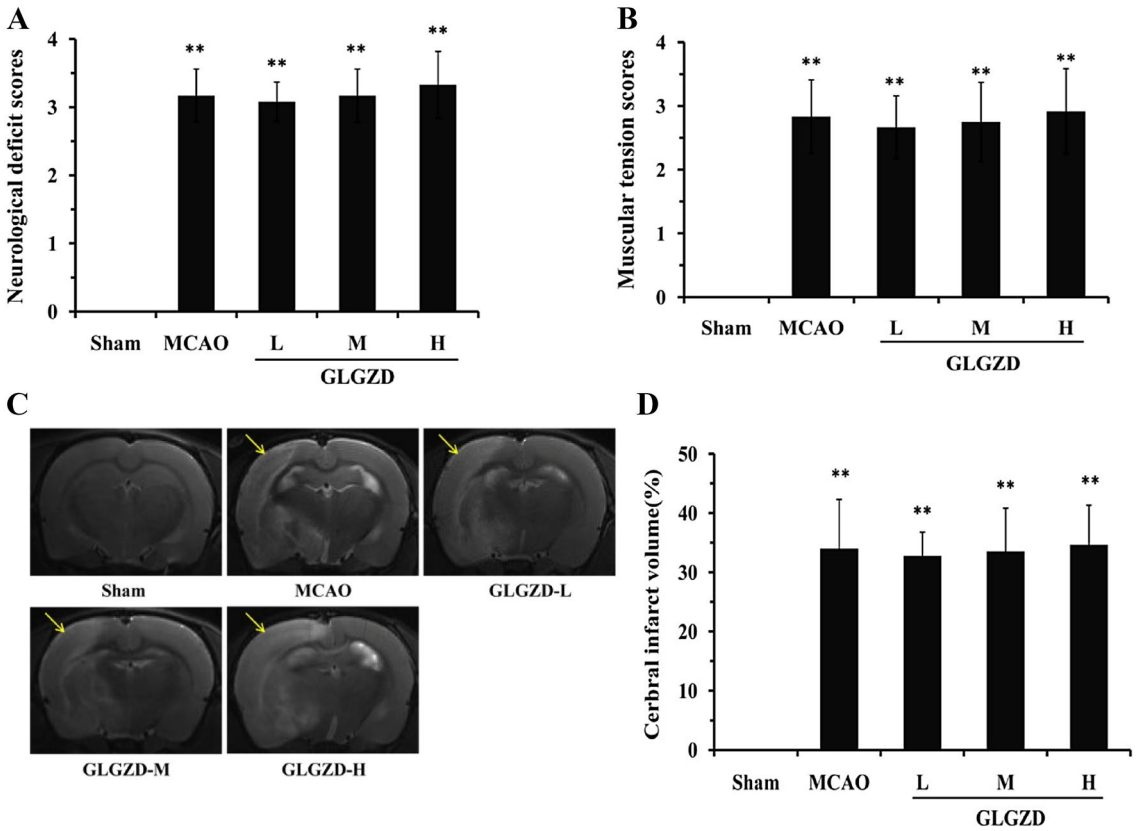

Fig. 2 The neurological deficit score, muscle tension score and cerebral infarction volume in MCAO-injured rats before GLGZD treatment. **a** Neurological function scores of rats after surgery in each group (n = 12). **b** Muscle tension scores of rats in each group after surgery (n = 12). **c** T2-weighted MR images of rats after surgery. T2WI signals were abnormally high in the ischemic infarction area and turned out to be white, indicated with yellow arrows. **d** Cerebral infarction volume in rats in each group after surgery (n = 12). All data are expressed as the mean ± SD. $^{**}P < 0.01$ versus the sham group

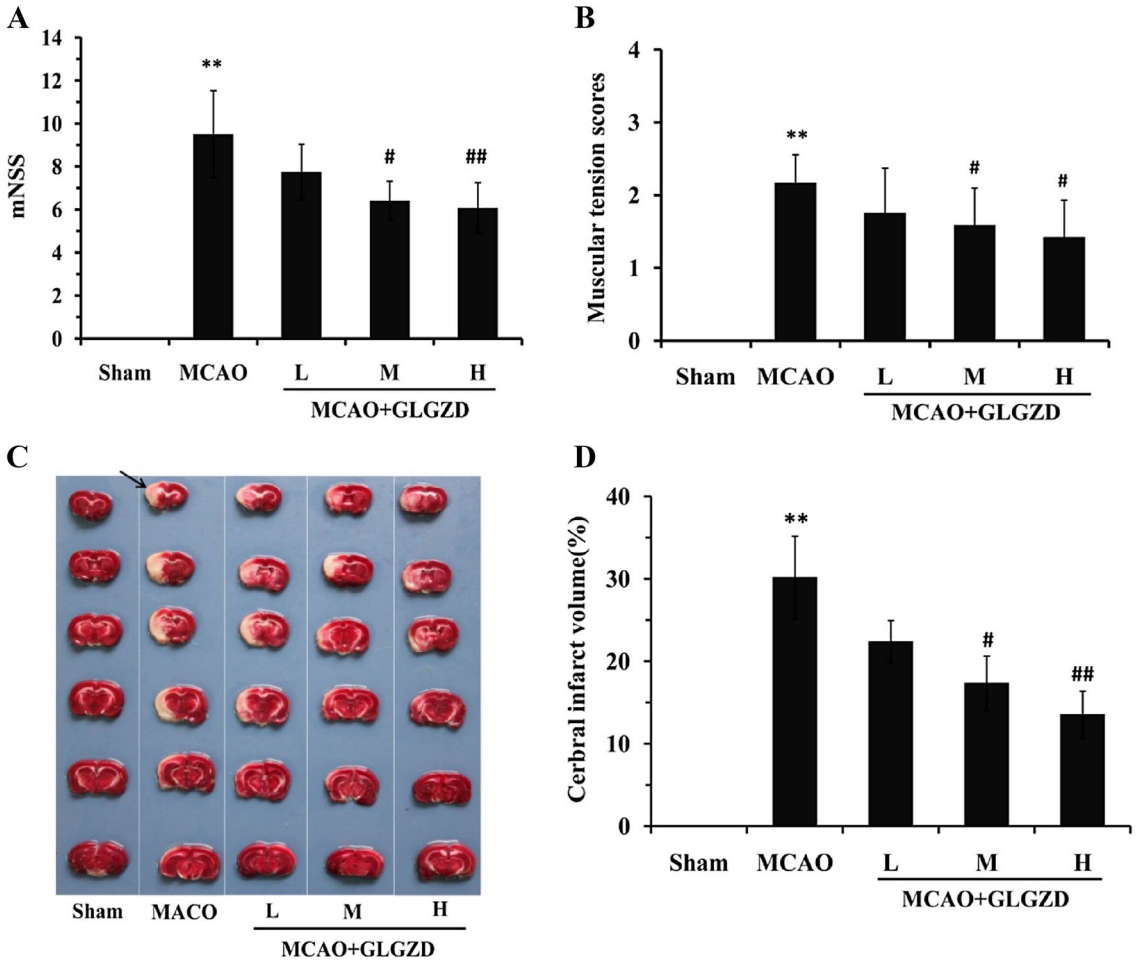

Fig. 3 Effects of GLGZD on nerve function damage, muscle tension and ischemic cerebral infarction volume in MCAO-injured rats. SD rats with ischemic stroke were administered a low dose (GLGZD-L, 3.6 g/kg), middle dose (GLGZD-M, 7.2 g/kg) or high dose (GLGZD-H, 14.4 g/kg) of GLGZD. Then, neurological function scoring, muscle tension scoring and TTC staining were performed. **a** Modified neurological severity score(mNSS) of rats in each group (n = 12). **b** Muscle tension scores of rats in each group (n = 12). **c** TTC-stained cerebral slices in each group (n = 6), with black arrows indicating the "infarct zone". **d** Quantitative analysis of the cerebral infarction volume. All data are expressed as the mean ± SD. $^{**}P < 0.01$ versus the sham group; $^{\#}P < 0.05$, $^{\#\#}P < 0.01$ versus the MCAO group

Effects of GLGZD on Motor Function of MCAO-Injured Rats

CatWalk gait analysis (Fig. 4a–d) showed that MCAO-injured rats with hemiplegiain the right limb had significant differences. Compared with the sham group, the MCAO group exhibited significantly decreased run average speed, print area in the right limb and stride length ($P < 0.05$), and significantly increased run duration of MCAO animals was significantly increased ($P < 0.01$). GLGZD significantly improved the run average speed, print area and stride length, and decreased the run duration in MCAO rats ($P < 0.05$, 0.01).

Effects of GLGZD on the Cerebral Pathological State in the Ischemic Motor Cortex

HE staining (Fig. 5) showed that there were no obvious pathological changes in the cerebral motor cortical neurons of rats in the sham group. The cells were arranged neatly, their outlines were evident, and their coloration was uniform; the cell membranes were intact, the nuclei and nucleoli were clearly observed, and the cytoplasm of each cell was abundant. Additionally, there was no edema or inflammatory cell infiltration in the tissues. In the MCAO model group, a large number of cells were degenerated and necrotic. The cells were arranged in a disorderly pattern, the gap between

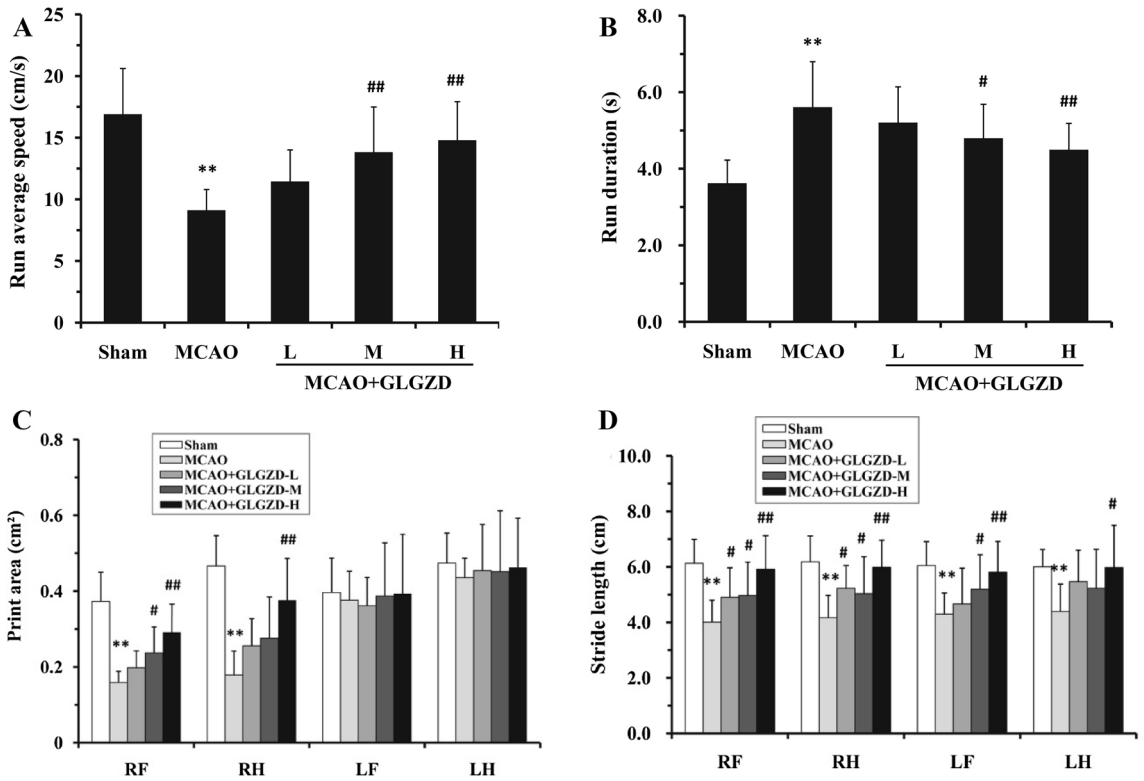

Fig. 4 Effects of GLGZD on motor function in MCAO-injured rats. The run average speed, print area, stride length and run duration of rats were detected using the CatWalk gait analysis system. Quantification and analysis of these parameters was used to assess motor function of rat limbs. **a** The run average speed of rats in each group. **b** The run duration of rats in each group. **c** The print area of rats in each group. **d** The stride length of rats in each group. *RF* right forelimb, *RH* right hindlimb, *LF* left forelimb, *LH* left hindlimb. All data are expressed as the mean ± SD. $^{**}P < 0.01$ versus the sham group; $^{\#}P < 0.05$, $^{\#\#}P < 0.01$ versus the MCAO group

cells was widened, the structure was slightly loose, the morphology was abnormal and irregular, the cell bodies were shrunken, the cytoplasm was agglomerated, the nuclei were condensed and stained, and some cells had unclear boundaries. Inflammatory cell infiltration and interstitial edema were obvious. After GLGZD administration, the pathological state was significantly improved compared with that in the MCAO model group, and the degree of necrosis and number of necrotic cells were significantly reduced.

Effects of GLGZD on Number of Nissl-Positive Cells in the Ischemic Motor Cortex

Nissl staining (Fig. 6a–c) showed that the motor cortical neurons in the sham group were arranged neatly. The membrane was blue-violet, the nucleus was pale blue, and many Nissl bodies were observed. In the MCAO group, the morphology of motor cortical neurons was characterized by obvious swelling, light staining, disordered arrangement, cell atrophy, deep nuclear staining, increased intercellular space, and a disappearance of or decrease in Nissl body corpuscles. Compared with the sham group, the MCAO group had significantly fewer Nissl-positive cells (normal neurons) ($P < 0.01$). After middle- and high-dose GLGZD treatment, the cell swelling was significantly lightened, the number of necrotic cells was significantly reduced, and the number of Nissl bodies was increased much more than that of MCAO alone ($P < 0.01$).

Effects of GLGZD on Cell Apoptosis in the Ischemic Cerebral Motor Cortex of MCAO-Injured Rats

TUNEL staining (Fig. 7a–c) showed that the number of TUNEL-positive cells in the cerebral motor cortex in the MCAO group was significantly increased compared with that in the sham operation group ($P < 0.01$), which indicated that cell apoptosis in the motor cortical injury area was significantly enhanced after MCAO. Compared with the MCAO group, the GLGZD groups had a significantly reduced number of apoptotic cells in the cerebral motor cortex ($P < 0.05, 0.01$).

Effects of GLGZD on the Protein Expression of PARP-1, PAR, AIF, Endo G and Hsp70 in the Ischemic Cortex of MCAO-Injured Rats

Figure 8a, b shows that the total protein expression of PARP-1, AIF, PAR and Endo G in the ischemic cortex of the

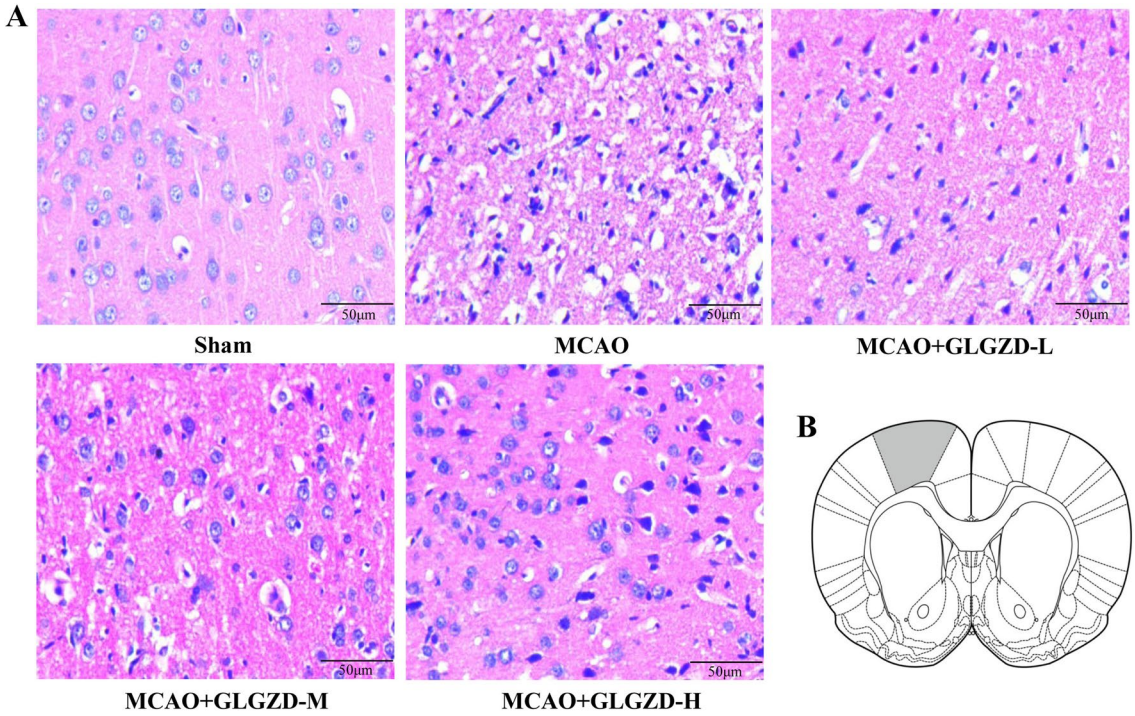

Fig. 5 Effects of GLGZD on the cerebral pathological changes in the ischemic cortex. **a** Histopathological picture of the rat motor cortex stained with HE (×200). Large amount of degeneration and necrosis of neuron were observed in the brain tissue in the ischemic motor cortex of MACO rats. The cells were arranged in a disorderly pattern, the gap between cells was widened, the structure was slightly loose, the morphology was abnormal and irregular, the cell bodies were shrunken, the cytoplasm was agglomerated. Inflammatory cell infiltration and interstitial edema were obvious. After GLGZD administration, the pathological state was significantly improved compared with that in the MCAO model group. **b** A map of the rat brain [24], with the motor cortex marked ingray

MCAO group was significantly higher than that of the sham group ($P<0.01$). Conversely, the total protein expression of Hsp70 was observed to be significantly reduced ($P<0.01$). After GLGZD treatment, the total protein expression levels of PARP-1, PAR, AIF and Endo G were significantly lower than those of MCAO alone, and the expression of total Hsp70 protein was significantly increased ($P<0.05$ or 0.01).

Figure 8c, d shows that compared with the sham group, the MCAO group showed significantly increased expression of PARP-1, AIF and Endo G protein in the nucleus of the ischemic cortex ($P<0.01$), and the PAR protein expression was significantly reduced ($P<0.01$). Compared with that in the MCAO group, the expression of PAR protein in the nucleus of the ischemic cortex of the GLGZD-H group was significantly increased, while the expression of PARP-1, AIF and Endo G protein in the nucleus was significantly less than that in the MCAO group ($P<0.05$, 0.01).

Figure 8e, f shows that the mitochondrial protein expression of PAR in the ischemic cortex of the MCAO group was significantly increased compared with that in the sham group ($P<0.05$), while the mitochondrial expression of AIF and Endo G protein was significantly decreased ($P<0.01$). Compared with the MCAO group, the GLGZD-H group had significantly upregulated expression of AIF and Endo G protein in mitochondria and decreased expression of PAR protein in mitochondria ($P<0.01$).

Effects of GLGZD on the PARP-1 Labeled Cells in the Ischemic Brain Motor Cortex of Rats with MCAO

The immunofluorescence results (Fig. 9a–c) showed that the expression of PARP-1 protein in the nucleus of the ischemic motor cortex of the MCAO group was significantly higher than that of the sham group ($P<0.01$), suggesting that cerebral ischemic injury had occurred. The overexpression of PARP-1 in the nucleus triggered downstream signaling cascades and led to non-caspase-dependent apoptosis. The expression of PARP-1 protein in the nucleus of the GLGZD group was significantly lower than that of the MCAO group ($P<0.05$, 0.01).

Discussion

Animal models of global and focal cerebral ischemia are frequently applied in the experimental study of cerebral ischemia–reperfusion injury. However, the main type

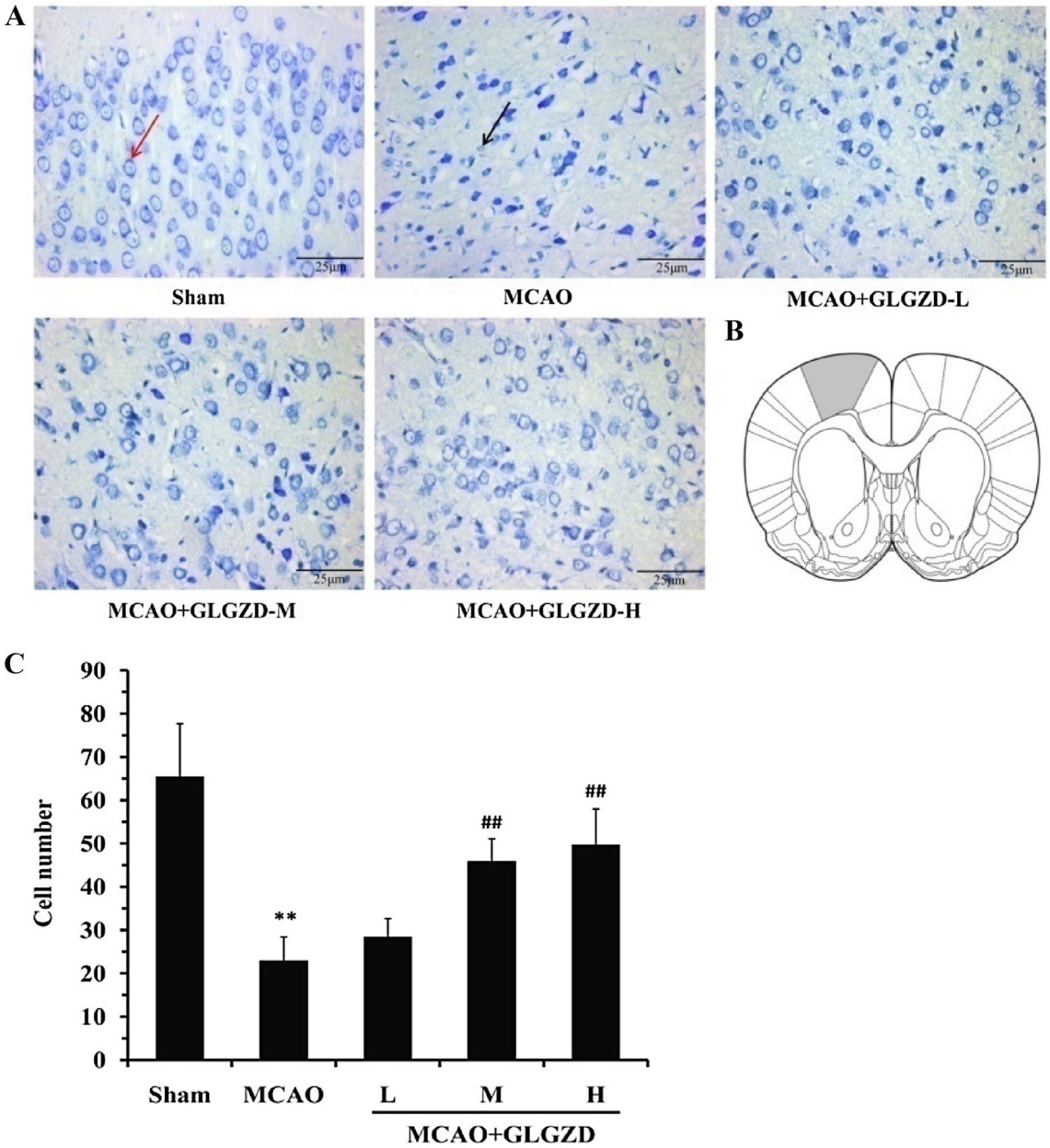

Fig. 6 Effects of GLGZD on thenumber of Nissl-positive cells in the ischemic cortex. **a** Morphological picture of neurons in rat motor cortical tissue stained with Nissl (×400); the red arrow indicates a purple-blue Nissl body in normal neurons, and the black arrow indicates that Nissl bodies were dissolved and disappeared (or decreased in number) among the injured neurons. **b** A map of the rat brain, with the motor cortex marked ingray. **c** The number of Nissl-positive cells (i.e., intact neurons). All data are expressed as the mean ± SD. $^{**}P < 0.01$ versus the sham group; $^{\#\#}P < 0.01$ versus the MCAO group

of injury found in the clinic is focal cerebral ischemia. MCAO causes focal cerebral ischemia in animals without craniotomy and reduces the risk of intracranial infection. Therefore, it is a highly repeatable and reliable method for the further research [25]. Moreover, MCAO can adequately mimic clinical cerebral ischemic diseases and is regarded as a classic model for studying ischemic stroke [26, 27]. Limb spasticity after stroke is currently believed to be caused by upper motor neuron injury after cerebral ischemia. The injury of upper motor neurons induced the dissimilation of the central nervous system inhibition of the spinal cord, leading to the release of the primitive functions of the lower centers, increased excitability of the motor circuit, and an overly strong skeletal muscle stretch reflex, finally resulting in increased muscle tension in the limb of the affected side, and the presentation of a spasmodic state [28]. In our study, blocking the blood flow of the middle cerebral artery in rats with a thread bolt

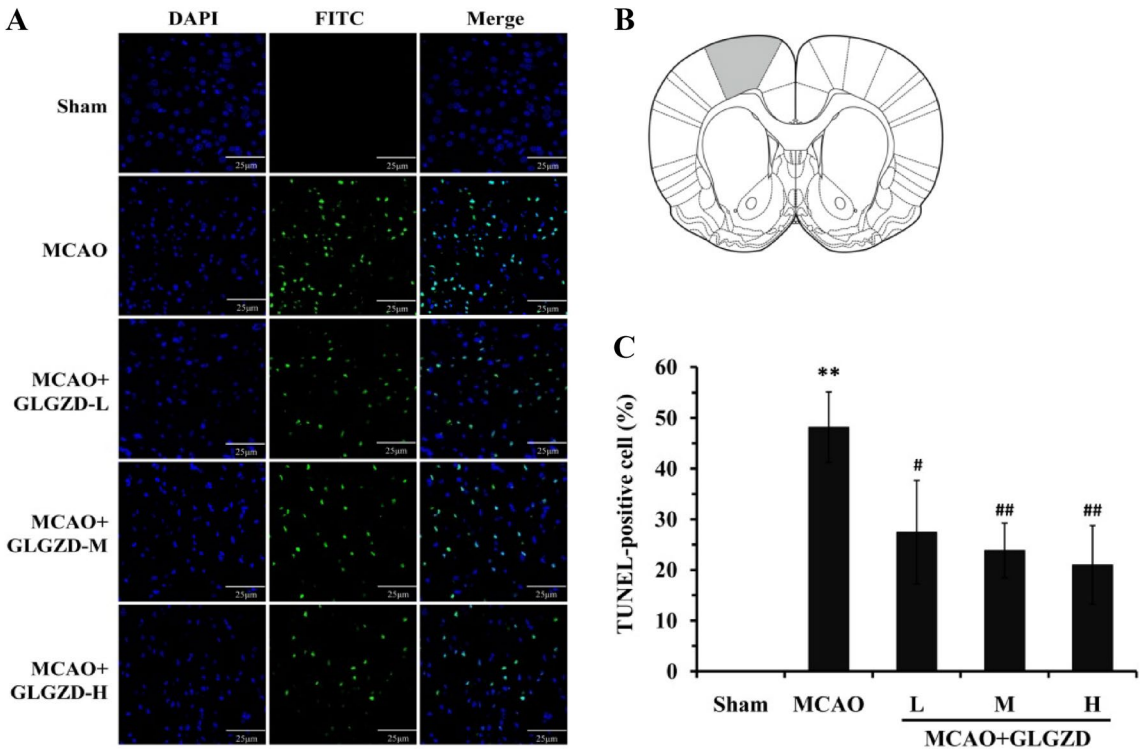

Fig. 7 Effects of GLGZD on cell apoptosis in the ischemic cerebral motor cortex of MCAO-injured rats. The cells presented blue fluorescence after DAPI staining. The apoptotic cells exhibited green fluorescence after TUNEL staining. The TUNEL-positive expression rate = (the number of TUNEL-positive cells/the number of cells stained by DAPI) × 100%. **a** The morphology of apoptotic cells (×400) under laser confocal microscopy after TUNEL staining. **b** A map of the rat brain, with the motor cortex marked in gray. **c** Results of the TUNEL-positive cell analysis. All data are expressed as the mean ± SD. $^{**}P < 0.01$ versus the sham group; $^{\#}P < 0.05$, $^{\#\#}P < 0.01$ versus the MCAO group (Color figure online)

caused obvious symptoms of nerve function defects: the rats turned or dumped toward the side opposite from the injury when they walked, or were even unable to walk. Furthermore, compared to the sham group, the MCAO group exhibited a significantly larger cerebral infarction area and obviously increased muscle tension of the contralateral limb, with a muscle tension score > 1, suggesting that the limb-spasm rat model of MCAO was successfully established.

Hemiplegic gait is one of the most common symptoms caused by stroke. Gait abnormalities are the most obvious manifestation of limb movement dysfunction and the external manifestation of nerve function injury. The Catwalk XT gait analysis system works based on an interaction of pressure and fluorescence to efficiently visualize the prints and calculate statistics. The CatWalk gait analysis showed that the print area of the right limb of MCAO model rats was significantly lower than that of the sham group rats, suggesting that ischemia–reperfusion of the middle cerebral artery damaged the motor cortex around the middle cerebral artery and affected the control of the plantar surface of the limbs in rats. The decreased run average speed, stride length and increased run duration of rats in the MCAO group indicated that the motor function of rats decreased after cerebral ischemia injury.

After GLGZD treatment for 7 days, the mNSS of rats in the MCAO group significantly decreased ($P < 0.05$, 0.01), and the motor, sensory, reflex and balance functions significantly improved. GLGZD treatment also decreased the muscle tension on the affected side of rats, relieved limb spasticity status, and improved the gait parameters ($P < 0.05$, 0.01), suggesting that the treatment promoted the recovery of motor function after cerebral ischemia.

In our experiments, TTC staining, HE staining and Nissl staining were also used to comprehensively evaluated the therapeutic effects of GLGZD. The results of TTC staining and HE staining showed that GLGZD significantly reduced the cerebral infarction volume caused by cerebral ischemia ($P < 0.05$, 0.01) and significantly improved the pathological state of neurons in the ischemic motor cortex.

The number and morphological characteristics of neurons can reflect their growth and development, their transport of substances and the normal function of their activities. The Nissl staining results showed that cerebral ischemia–reperfusion injury can cause Nissl body injury ($P < 0.01$). GLGZD treatment obviously protected the

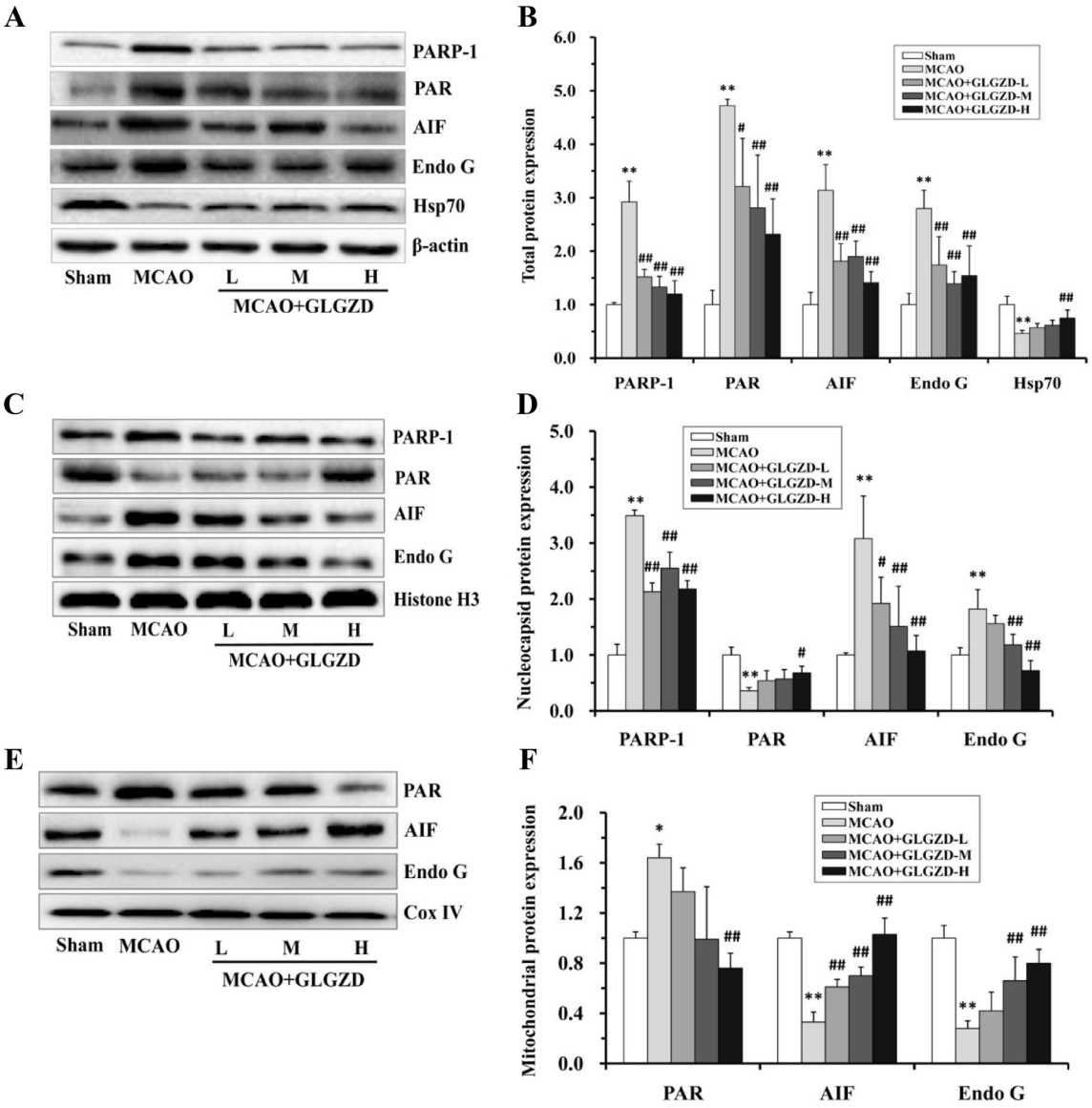

Fig. 8 Effects of GLGZD on the expression of PARP-1/AIF signaling pathway-related proteins in the ischemic brain of rats with MCAO. **a**, **b** Relative optical density analysis of the total protein expression of PARP-1, PAR, AIF, Endo G and Hsp70. β-actin was used as the internal control. **c**, **d** Relative optical density analysis of the nucleoprotein expression of PARP-1, PAR, AIF, and Endo G. Histone H3 was used as the internal control. **e**, **f** Relative optical density analysis of the mitochondrial protein expression of PAR, AIF, and Endo G. Cox IV was used as the internal control. All data are expressed as the mean ± SD. $^{*}P<0.05$, $^{**}P<0.01$ versus the sham group; $^{\#}P<0.05$, $^{\#\#}P<0.01$ versus the MCAO group

neurons and effectively inhibited the Nissl body injury in the ischemic motor cortex ($P<0.01$).

Apoptosis is a genetically controlled cell death program that is reversible. The results of TUNEL staining showed that the apoptotic cells in the MCAO group were significantly increased compared with those in the sham group ($P<0.01$), and the apoptotic cells with green fluorescence were mainly located in the ischemic penumbra. GLGZD treatment significantly inhibited the apoptosis of neurons in the ischemic motor cortex ($P<0.05$ or 0.01) and exerted neuroprotective effects.

Apoptosis is a genetically regulated form of cell death (programmed cell death) that can be divided into two major types: caspase-dependent cell death and non-caspase-dependent cell death. Studies have shown that apoptosis mediated by the PARP-1/AIF signaling pathway is non-caspase-dependent. PARP-1 is an intracellular enzyme of the PARP family that has been studied widely. PARP-1 is

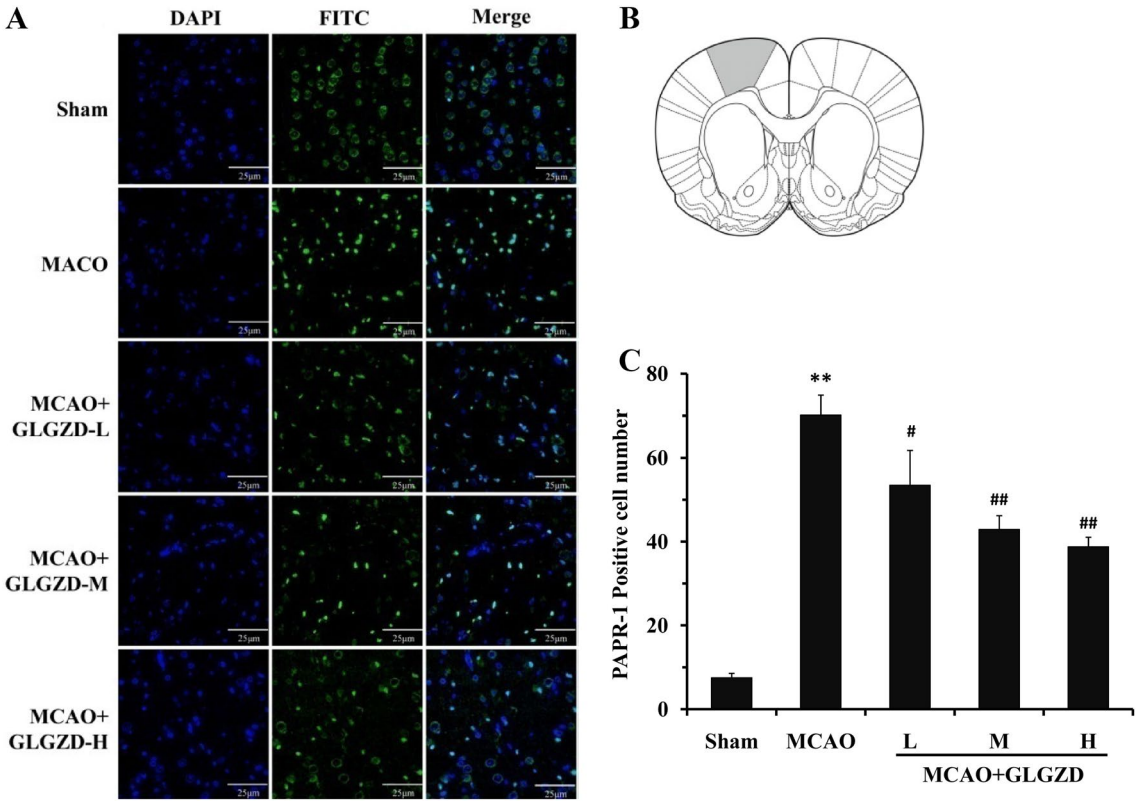

Fig. 9 Effects of GLGZD on the PARP-1 labeled cells in the ischemic brain motor cortex of rats with MCAO. **a** Immunofluorescence analysis examining the location and expression of PARP-1 protein, counterstained with DAPI (×400). **b** A map of the rat brain, with the motor cortex marked in gray. **c** Analysis of PARP-1-positive cells. All data are expressed as the mean ± SD. $^{**}P < 0.01$ versus the sham group; $^{\#}P < 0.05$, $^{\#\#}P < 0.01$ versus the MCAO group

an important nuclear protease that maintains intracellular balance, accounting for more than 90% of all intracellular PARP activity. Overactivation of PARP-1 is a common terminal process mediating cell death. Moreover, PARP-1 overactivation is closely related to the occurrence of stroke [29–32]. PARP-1 is a catalytic enzyme for PAR synthesis. Under physiological conditions or mild ischemia, PARP-1 can be activated by DNA fragments and bind to damaged DNA, which decomposes nicotinamide adenine dinucleotide into adenosine diphosphate-ribose and nicotinamide. Then, catalytic polymerization occurs after the substrate adenosine diphosphate-ribose binds to the receptor protein and generates PAR. Negatively charged PAR can covalently bind to various nuclear proteins such as histones and transcription factors, repair damaged DNA, and enable neurons to survive by tolerating ischemia. When ischemic damage is severe, DNA damage causes PARP-1 overactivation and increased PAR production [33]. Altering protein–protein and protein-DNA interactions leads to a series of cascade reactions, including phosphatidylserine ectropion, mitochondrial membrane potential dissipation, translocation of PAR to mitochondria, which induces the AIF release and then translocated to the nucleus, this lead to extensive production of large-scale DNA fragments and chromatin condensation, eventually causing apoptosis and death [34].

AIF is an oxidoreductase located in the mitochondrial membrane space and is considered a scavenger of reactive oxygen species (ROS). It has the dual role of maintaining normal mitochondria and inducing cell death [35, 36]. In the process of parthanatos, AIF acts as an important mediator in the production of chromosome condensation and large fragmentation of the DNA in the nucleus. Lee found that AIF and Endo G are translocated from mitochondria to the nucleus almost at the same time after ischemic stroke [37], and the interaction between the two proteins causes damage in the DNA ladder pattern, chromosome condensation, and secondary induction of PARP-1 expression, thereby catalyzing the PAR response as well as accelerating cell apoptosis.

In the present study, the expression of PARP-1 protein was detected by Western blotting and immunofluorescence histochemistry. The results showed that the total protein and nucleoprotein expression levels of PARP-1 in the MCAO group were significantly higher than those in the sham group ($P < 0.01$). After GLGZD treatment, the total protein and nucleoprotein expression in PARP-1 was significantly reduced ($P < 0.05$, 0.01) compared with that of MCAO

alone. These findings suggest that the effects of GLGZD on neuronal apoptosis-induced by cerebral ischemia–reperfusion injury are related to the inhibition of excessive activation of PARP-1.

The results of the Western blot analysis showed that the total protein expression of PAR, AIF and Endo G in the ischemic cortex of MCAO-injured rats was increased significantly ($P < 0.01$) compared with that in the sham-operated rats. The mitochondrial protein expression of PAR and the nucleoprotein expression of AIF and Endo G were significantly increased in the MCAO group compared with the sham group ($P < 0.05$, 0.01), while the nucleoprotein expression of PAR and the mitochondrial protein expression of AIF and Endo G were significantly decreased in the MCAO compared with the sham group ($P < 0.01$). The results mentioned above suggest that overexpression of the PARP-1 protein in the nucleus leads to increased synthesis of PAR during cerebral ischemia–reperfusion injury as well as increased translocation of PAR into mitochondria, which induces the release of AIF and Endo G and their subsequent translocation to the nucleus, resulting in apoptosis. After GLGZD treatment for 7 days, the total protein expression of PAR, AIF and Endo G was significantly decreased compared with that of MCAO alone ($P < 0.05$, 0.01). The expression of the protein PAR in mitochondria and the protein AIF and Endo G in nucleus was measured and found to be significantly decreased ($P < 0.05$, 0.01) in the GLGZD group compared with the MCAO group; the nucleoprotein expression of PAR and the mitochondrial protein expression of AIF and Endo G were significantly higher in the GLGZD group than in the MCAO group ($P < 0.05$, 0.01).

These results suggest that GLGZD can inhibit the expression of PARP-1, reduce PAR synthesis and inhibit PAR translocation into mitochondria, thereby reducing the release of AIF and Endo G and inhibiting the translocation of AIF and Endo G from mitochondria to the nucleus. Finally, GLGZD exerts its neuroprotective effects by inhibiting ischemia-induced neuronal apoptosis.

Although no inhibitors currently block AIF-induced chromosome condensation and large-scale DNA fragmentation, Hsp70 can inhibit AIF migration and retain AIF in the cytoplasm [38]. The Western blot results in our study showed that the protein expression of Hsp70 in the ischemic cortex of the MCAO group was significantly decreased compared with that of the sham group ($P < 0.01$). After GLGZD treatment for 7 days, the protein expression of Hsp70 was significantly increased compared with that of MCAO alone ($P < 0.01$), suggesting that GLGZD can promote the expression of Hsp70 protein and help to inhibit the translocation of AIF.

Due to the complexity of the compounds in traditional Chinese medicine, this study used HPLC to quantitatively analyze 26 main components of GLGZD to control the quality of GLGZD. Studies have shown that GLGZD contains citrulline [39], gallic acid [40], protocatechuic acid [41], paeoniflorin [42–44], glycyrrhizin [45], glycyrrhizic acid [46], isoliquiritigenin [47], 6-gingerol [48], curcumin [49] and other ingredients that have protective effects against brain damage after ischemia/reperfusion injury. These results suggest that GLGZD exerts its protective effects via those components. In this study, HPLC was used to analyze the components in GLGZD to obtain a fingerprint, which also laid the foundation for further research on the quality control and pharmacodynamic basis of GLGZD.

Conclusions

In summary, GLGZD significantly reduced the infarct area of MCAO rats and rescued the neurons of ischemic lateral motor cortex from pathological status, thereby promoting the recovery of nerve and motor function after cerebral ischemia, relieving limb spasticity status, and resulting in a strong protective effect against ischemia–reperfusion damage, and its effects are associated with the regulation of the expression and translocation of PARP-1/AIF pathway-related proteins and the further suppression of ischemia-induced neuronal apoptosis.

Acknowledgements This study was funded by the National Natural Science Foundation of China (Grant No. 81873031) and the Natural Science Foundation of Fujian Science and Technology Department (Grant No. 2017J01837).

Compliance with Ethical Standards

Conflict of interest All authors declare no conflict of interest.

References

1. Huang R (2010) Neurology, vol 1. Beijing Higher Education Press, Beijing, p 639
2. Ji R, Schwamm LH, Pervez MA, Singhal AB (2013) Ischemic stroke and transient ischemic attack in young adults: risk factors, diagnostic yield, neuroimaging, and thrombolysis. JAMA Neurol 70:51–57
3. Elovic E (2001) Principles of pharmaceutical management of spastic hypertonia. Phys Med Rehabil Clin N Am 12:793–816
4. Gong W, Zhang T, Sun X (2008) Advancein spasticity after stroke. Chin J Rehabil Theory Pract 14:212–213
5. Li Y, Chopp M, Jiang N, Yao F, Zaloga C (1995) Temporal profile of in situ DNA fragmentation after transient middle cerebral artery occlusion in the rat. J Cereb Blood Flow Metab 15:389–397
6. Ferrer I, Planas AM (2003) Signaling of cell death and cell survival following focal cerebral ischemia: life and death struggle in the penumbra. J Neuropathol Exp Neurol 62:329–339
7. Saito A, Maier CM, Narasimhan P, Nishi T, Song YS, Yu F, Liu J, Lee Y, Nito C, Kamada H, Dodd RL, Hsieh LB, Hassid B, Kim EK, González M, Chan PK (2005) Oxidative stress and neuronal

death/survival signaling in cerebral ischemia. Mol Neurobiol 31:105–116
8. Zhang F, Yin W, Chen J (2004) Apoptosis in cerebral ischemia: executional and regulatory signaling mechanisms. Neurol Res 26:835–845
9. Radak D, Katsiki N, Resanovic I, Jovanovic A, Sudar-Milovanovic E, Zafirovic S, Mousa S, Isenovi E (2017) Apoptosis and acute brain ischemia in ischemic stroke. Curr Vasc Pharmacol 15:1–20
10. Khoshnam SE, Winlow W, Farzaneh M, Farbood Y, Moghaddam HF (2017) Pathogenic mechanisms following ischemic stroke. Neurological Sciences 38:1167–1186
11. Harraz MM, Dawson TM, Dawson VL (2008) Advances in neuronal cell death 2007. Stroke 39:286–288
12. Langelier MF, Planck JL, Roy S, Pascal JM (2012) Structural basis for dna damage-dependent poly(adp-ribosyl)ation by human parp-1. Science 336:728–732
13. Poitras MF, Koh DW, Yu SW, Andrabi SA, Mandir AS, Poirier GG, Dawson VL, Dawson TM (2007) Spatial and functional relationship between poly(ADP-ribose) polymerase-1 and poly(ADP-ribose) glycohydrolase in the brain. Neuroscience 148:198–211
14. Yang C, Chen L, Tao J (2012) New usage of a classical formula-Gua Lou Gui Zhi decoction. Liaoning Zhong Yi Za Zhi 39:166–167
15. Chen Y, Chen L, Tao J (2013) Clinical research on treating limbs spasm from cerebral apoplexy with the Gualou Guizhi decoction. Clin J Chin Med 5:7–9
16. Zhang Y, Li H, Huang M, Chu K, Xu W, Zhang S, Que J, Chen L (2014) Neuroprotective effects of Gualou Guizhi decoction in vivo and in vitro. J Ethnopharmacol 158:76–84
17. Chen X, Li H, Huang M, Huang M, Xu W, Chu K, Chen L, Zhang Y (2014) Effect of Gua Lou Gui Zhi decoction on focal cerebral ischemia-reperfusion injury through regulating the expression of excitatory amino acids and their receptors. Molecular Medicine Reports 10:248–254
18. Huang J, Tao J, Xue X, Yang S, Han P, Lin Z, Xu W, Lin J, Peng J, Chen L (2013) Gua Lou Gui Zhi decoction exerts neuroprotective effects on post-stroke spasticity via the modulation of glutamate levels and AMPA receptor expression. Int J Mol Med 31:841–848
19. Nan L, Yang L, Zheng Y, He Y, Xie Q, Chen Z, Li H, Huang M (2017) Effects of Gualou Guizhi decoction aqueous extract on axonal regeneration in organotypic cortical slice culture after oxygen-glucose deprivation. Evid Based Complement Alternat Med 2017:1–11
20. Zhang S, Zhang Y, Huang L, Wei X, Chu K, Chen L, Chen X (2015) Antioxidant and anti-excitotoxicity effect of Gualou Guizhi decoction on cerebral ischemia/reperfusion injury in rats. Exp Ther Med 9:2121–2126
21. Ashworth B (1964) Preliminary trial of carioproda in multiple sclerosis. Practitioner 19:540
22. Longa EZ, Weinstein PR, Carlson S, Cummins R (1989) Reversible middle cerebral artery occlusion without craniotomy in rats. Stroke 20:84–91
23. Wen Z, Xu X, Xu L, Yang L, Xu X, Zhu J, Wu L, Jiang Y, Liu X (2017) Optimization of behavioural tests for the prediction of outcomes in mouse models of focal middle cerebral artery occlusion. Brain Res 1665:88–94
24. Paxinos G, Watson C (2007) The rat brain in stereotaxic coordinates, 6th edn. Academic Press, San Diego
25. Liu F, McCullough LD (2011) Middle cerebral artery occlusion models in rodents: methods and potential pitfalls. Bio Med Res Inter 2011:464701
26. Fujimoto M, Takagi Y, Aoki T, Hayase M, Marumo T, Gomi M, Nishimura M, Kataoka H, Hashimoto N, Nozaki K (2008) Tissue inhibitor of metalloproteinases protect blood–brain barrier disruption in focal cerebral ischemia. J Cereb Blood Flow Metab 28(10):1674–1685
27. Goldstein LB (2007) Acute ischemic stroke treatment in 2007. Circulation 116:1504–1514
28. Esquenazi A, Talaty M (2000) Gait analysis: technology and clinical applications. In: Braddom R (ed) Physical medicine and rehabilitation. WB Saunders Company, Philadelphia, pp 93–108
29. David KK, Andrabi SA, Dawson TM, Dawson VL (2009) Parthanatos, a messenger of death. Front Biosci 14:1116–1128
30. Park EM, Cho S, Frys K, Racchumi G, Zhou P, Anrather J, Iadecola C (2004) Interaction between inducible nitric oxide synthase and poly(ADP-ribose) polymerase in focal ischemic brain injury. Stroke 35:2896–2901
31. Amé JC, Spenlehauer C, Murcia G (2004) The PARP superfamily. BioEssays 26:882–893
32. Fatokun AA, Dawson VL, Dawson TM (2014) Parthanatos: mitochondrial-linked mechanisms and therapeutic opportunities. Br J Pharmacol 171:2000–2016
33. Fouquerel E, Sobol RW (2014) ARTD1 (PARP1) activation and NAD+ in DNA repair and cell death. DNA Repair 23:27–32
34. Hassa PO, Haenni SS, Elser M, Hottiger MO (2006) Nuclear ADP-ribosylation reactions in mammalian cells: where are we today and where are we going? Microbiol Mol Biol Rev 70:789–829
35. Ishitsuka K, Hideshima T, Hamasaki M, Raje N, Kumar S, Podar K, Gouill SL, Shiraishi N, Yasui H, Roccaro AM, Tai YZ, Chauhan D, Fram R, Tamura K, Jain J, Anderson KC (2005) Novel inosine monophosphate dehydrogenase inhibitor VX-944 induces apoptosis in multiple myeloma cells primarily via caspase-independent AIF/Endo G pathway. Oncogene 24:5888–5896
36. Lorenzo HK, Susin SA, Penninger J, Kroemer G (1999) Apoptosis inducing factor (AIF): a phylogenetically old, caspase-independent effector of cell death. Cell Death Differ 6:516–524
37. Lee BI, Lee DJ, Cho KJ, Kim GW (2005) Early nuclear translocation of endonuclease G and subsequent DNA fragmentation after transient focal cerebral ischemia in mice. Neurosci Lett 386:23–27
38. Matsumori Y, Hong SM, Aoyama K, Fan Y, Kayama T, Sheldon RA, Vexler ZS, Ferriero DM, Weinstein PR, Liu J (2005) Hsp70 overexpression sequesters AIF and reduces neonatal hypoxic/ischemic brain injury. J Cereb Blood Flow Metab 25:899–910
39. Chen W, Zhang S, Wang H (2011) Study of radices trichosanthis on neuronal apoptosis in rats with local cerebral ischemia reperfusion. Mod J Integr Tradit Chin West Med 20:1844–1845
40. Sun J, Ren DD, Wan JY, Chen C, Chen D, Yang H, Feng CL, Gao J (2017) Desensitizing mitochondrial permeability transition by ERK-cyclophilin D axis contributes to the neuroprotective effect of gallic acid against cerebral ischemia/reperfusion injury. Front Pharmacol 8:184
41. Kho AR, Choi BY, Lee SH, Hong DK, Lee SH, Jeong JH, Park KH, Song HK, Choi HC, Suh SW (2018) Effects of protocatechuic acid (PCA) on global cerebral ischemia-induced hippocampal neuronal death. Int J Mol Sci 19:1420
42. Guo RB, Wang GF, Zhao AP, Gu J, Sun XL, Hu G (2012) Paeoniflorin protects against ischemia-induced brain damages in rats via inhibiting MAPKs/NF-κB-mediated inflammatory responses. PLoS ONE 7:e49701
43. Zhang Y, Li H, Huang M, Chu K, Xu W, Zhang S, Que J, Chen L (2015) Paeoniflorin, a monoterpene glycoside, protects the brain from cerebral ischemic injury via inhibition of apoptosis. Am J Chin Med 43:543–557
44. He Y, Nan L, Huang M, Zheng Y, Yang L, Xu W, Chu K (2016) Paeoniflorin down-regulates the expression of NLRP1 and NLRP3 inflammasomes in rat hippocampal slices after oxygen-glucose deprivation. Int J Clin Exp Med 9:10907–10914
45. Gong G, Xiang L, Yuan L, Hu L, Wu W, Cai L, Yin L, Dong H (2014) Protective effect of glycyrrhizin, a direct HMGB1 inhibitor, on focal cerebral ischemia/reperfusion-induced inflammation, oxidative stress, and apoptosis in rats. PLoS ONE 9:e89450

46. Kim S, Jin Y, Shin JH, Kim ID, Lee HK, Park S, Han PL, Lee JK (2012) Glycyrrhizic acid affords robust neuroprotection in the postischemic brain via anti-inflammatory effect by inhibiting HMGB1 phosphorylation and secretion. Neurobiol Dis 46:147–156
47. Zhan C, Yang J (2006) Protective effects of isoliquiritigenin in transient middle cerebral artery occlusion-induced focal cerebral ischemia in rats. Pharmacol Res 53:303–309
48. Jiang Q, Xia B (2007) The anti-inflammatory effect of 6-gingerol on focal ischemia-reperfusion injury in rats. J Xianning Coll 47:197–201
49. Lei JR, Qin J, Jing Z, Huang KM, Rui FU, Zhou ZM (2010) Effects of curcumin on inflammatory reaction and blood-brain barrier permeability in rats following cerebral ischemic injury. Chin Pharmacol Bull 26:120–123